AD-A160 694 CALCULATION OF HELICOPTER AIRFOIL CHARACTERISTICS FOR HIGH TIP-SPEED APPLICATIONS(U) ARMY RESEARCH AND TECHNOLOGY LABS MOFFETT FIELD CA AEROMECHAN. . 1/1

UNCLASSIFIED W J MCCROSKEY ET AL. 17 MAY 85 F/G 20/4 NL

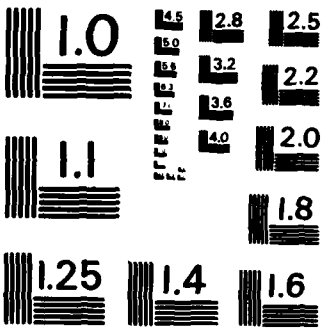

MICROCOPY RESOLUTION TEST CHART
NATIONAL BUREAU OF STANDARDS-1963-A

CALCULATION OF HELICOPTER AIRFOIL CHARACTERISTICS FOR HIGH TIP-SPEED APPLICATIONS

W.J. McCroskey, J.D. Baeder, and J.O. Bridgeman

NASA and U.S. Army Aeromechanics Laboratory (AVSCOM)
Ames Research Center, Moffett Field, California

PRESENTED AT THE 41st ANNUAL FORUM
OF THE
AMERICAN HELICOPTER SOCIETY
FT. WORTH, TEXAS
MAY 15-17, 1985

PAPER NO. _____

CALCULATION OF HELICOPTER AIRFOIL CHARACTERISTICS FOR HIGH TIP-SPEED APPLICATIONS

W. J. McCroskey, J. D. Baeder, and J. O. Bridgeman
Aeromechanics Laboratory, U.S. Army Research and Technology Laboratories (AVSCOM)
and NASA Ames Research Center, Moffett Field, California

Abstract

The aerodynamic section characteristics of several helicopter profiles have been computed using the Reynolds-averaged, thin-layer Navier-Stokes equations, and an eddy-viscosity model to approximate boundary-layer turbulence. The calculations were performed over a wide range of Mach numbers, angles of attack, and Reynolds numbers, with particular emphasis on transonic separated flow conditions that are relevant to advancing blades in high-speed forward flight. An extensive study was made of the accuracy of the numerical code, ARC2D, and of the sensitivity of the results to the numerical parameters and approximations. Also, comparisons were made with a large body of experimental data. The numerical results reproduce the measured airfoil behavior across the transonic regime, and the details of the computed flow field provide new insights into transonic airfoil behavior.

Symbols

C_D = drag coefficient

$\tilde{C}_D$ = transonic similarity drag parameter, Eq. (5)

C_L = lift coefficient

C_M = pitching moment coefficient about x/c = 0.25

C_p = pressure coefficient

C_p^* = sonic value of C_p

c = chord

E = flux vector, Eq. (1b)

e = total internal energy per unit volume

F = flux vector, Eq. (1b)

J = Jacobian of the coordinate transformation

M_∞ = free-stream Mach number

$\tilde{M}$ = transonic similarity Mach number parameter, Eq. (6)

Δn = mesh spacing normal to the airfoil in physical space

Pr = Prandtl number

p = pressure

Q = dependent variable vector, Eq. (1b)

Re = Reynolds number

S = viscous stress vector, Eq. (1c)

Δs = mesh spacing along the airfoil in physical space

t = time in Eqs. (1-3); also airfoil thickness in Eqs. (5,6)

U_∞ = free-stream velocity

U = contravariant velocity in the ξ-direction

u = x-component of velocity in physical space

V = contravariant velocity in the η-direction

v = y-component of velocity in physical space

x = horizontal coordinate in physical space

y = vertical coordinate in physical space

α = angle of attack, deg

Γ = circulation

γ = specific heat ratio

η = transformed coordinate normal to the airfoil surface

κ = thermal conductivity

μ = viscosity

ν_T = turbulent eddy viscosity

ξ = transformed coordinate along the airfoil surface

Presented at the 41st Annual Forum of the American Helicopter Society, Ft. Worth, Texas, May 15-17, 1985.

ρ = density

τ = time in computational space

Introduction

The transonic flow phenomena that occur on the advancing blade tips of modern helicopters have major effects on the aerodynamic performance, vibratory airloads, and acoustic radiation of the rotor. It is well known that under transonic conditions, the aerodynamic section characteristics, such as lift, drag, and pitching-moment coefficients, differ substantially from even the qualitative behavior of subsonic airfoils. Typical nonlinear behavior is illustrated in Fig. 1 from Ref. 1. Especially noteworthy are the various changes in the derivatives $dC_L/d\alpha$ and $dC_M/d\alpha$ as a function of Mach number.

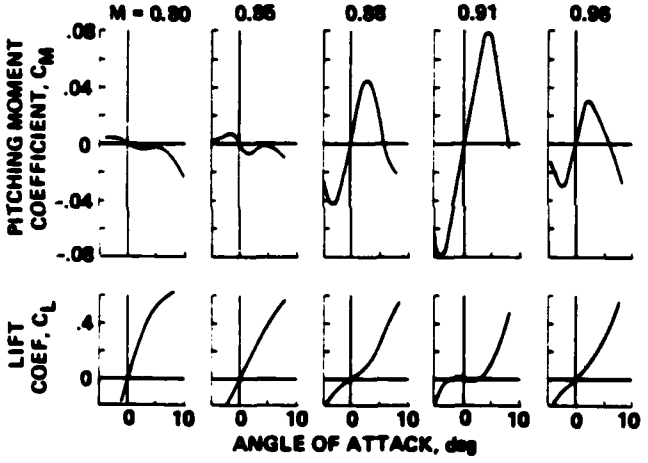

Fig. 1 Transonic Mach number characteristics of an NACA 0012 airfoil. (From Ref. 1.)

In general, airfoil C_L, C_D, and C_M depend primarily upon the geometry, Mach number, and angle of attack; and secondarily, upon Reynolds number, surface conditions, and free-stream turbulence. Heretofore, a complete set of nonlinear airfoil characteristics, such as those shown in Fig. 1, could only be obtained from expensive wind tunnel tests. However, the validity and accuracy of airfoil data can be tainted by wall interference, three-dimensional effects, and other factors, as indicated in Table 1. As a result of the various difficulties and uncertainties of transonic airfoil testing, results for the same model often differ more from one tunnel to another than from one airfoil section to another.[2-4]

This paper examines the extent to which an alternative tool, namely, modern Computational Fluid Dynamics (CFD) technology, can be used to derive useful, quantitative information about transonic airfoil characteristics. While CFD is free of most of the limitations of wind tunnel testing, it has its own shortcomings (cf. Table 2). As a result of the numerical approximations, computations from different numerical analyses are never in perfect accord, just as results from different facilities seldom agree.

Table 1 Limitations of wind tunnel testing

Primary
Wall interference
Three-dimensional effects
Costs
Model construction
Tunnel operations
Secondary
Free-stream turbulence
Nonuniform flow
Reynolds number limits
Geometry errors and model deformation
Measurement errors
Limited amount of data
Turn-around time

Table 2 Limitations of computational fluid dynamics

Primary
Turbulence model
Computer speed and memory
Costs
Code and software
Computer operations
Secondary
Transition model
Computational grids
Numerical errors
Turn-around time

The approach in this investigation is to solve the time-averaged, thin-layer Navier-Stokes equations with a simple eddy-viscosity model for the turbulent viscous layer next to the airfoil, using the NASA Ames Research Center CFD code ARC2D.[5-7] To our knowledge, this is the first attempt to apply such a sophisticated code to a wide range of practical airfoil cases. Therefore, our primary goals are: (1) to demonstrate that we

can reproduce the complex nonlinear behavior shown in Fig. 1, (2) to determine the physical processes of shock-wave development and viscous-inviscid interaction responsible for this behavior, and (3) to reduce the uncertainty surrounding quantitative transonic airfoil characteristics.

The specific objectives of this investigation were to obtain the lift, drag, and pitching-moment behavior for a conventional airfoil (e.g., the NACA 0012) and for a representative modern tip section (the Vertol VR-8) as functions of Mach number for the low-lift conditions that correspond to the advancing blade of a high-speed helicopter. Figure 2 shows the combinations of M_∞ and α for which calculations have been performed. Particular attention was given to the transonic regime above the drag-divergence Mach number; namely, $0.8 < M_\infty < 1.1$, where wind tunnel data are more limited and uncertain. The results in this regime were supplemented by calculations for NACA 0006 and 0015 profiles to study some effects of airfoil thickness. A limited number of reference calculations were also performed with the inviscid mode of ARC2D and with potential-flow codes.[8,9]

As indicated in Fig. 2, we have also calculated the section characteristics for some typical hover conditions, i.e., $0.5 < M_\infty < 0.6$, with particular emphasis on lift-to-drag ratios. On the other hand, we have avoided the conditions of retreating-blade stall, because we are skeptical that the current state of the art in turbulence modeling would permit such cases to be calculated with confidence.

Description of the Numerical Method

The computer code ARC2D (Refs. 5-7) developed at NASA Ames Research Center solves either the Euler equations or the thin-layer, Reynolds-averaged form of the Navier-Stokes equations with a relatively simple algebraic turbulence model, for two-dimensional steady or unsteady flow. The highlights of the method are outlined below; the details are documented in Refs. 5 and 6.

Governing Equations and Boundary Conditions

The two-dimensional equations of motion for a viscous perfect gas are written in strong conservation-law form in a generalized, body-fitted curvilinear coordinate system (ξ,η,τ), with the thin-shear-layer assumption for high-Reynolds-number turbulent flows, as described below.

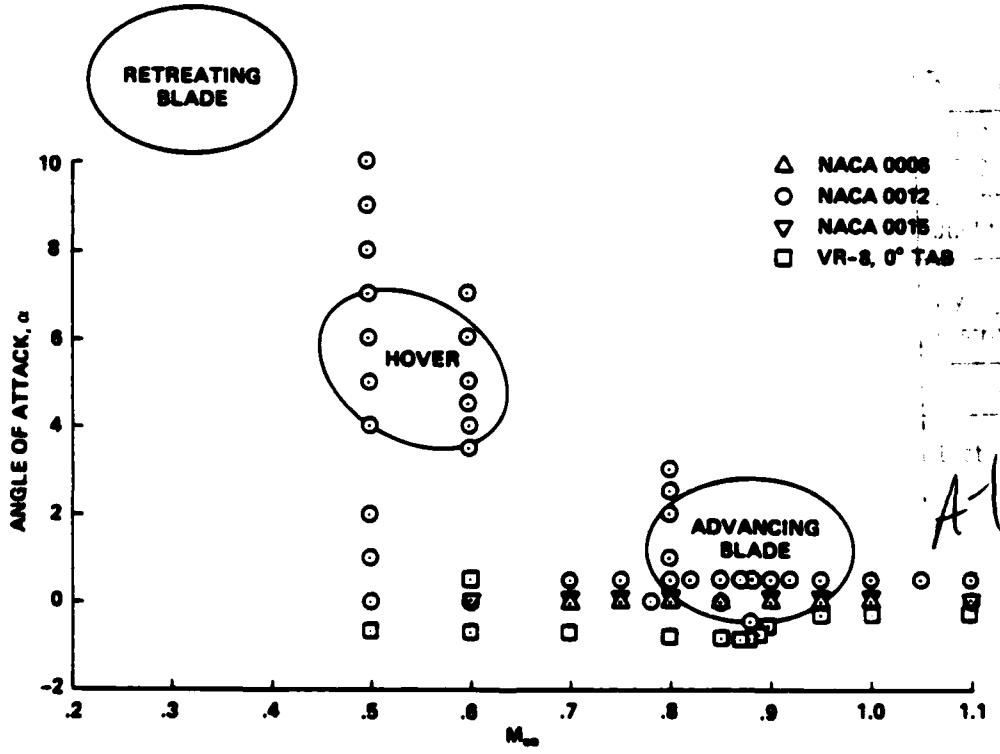

Fig. 2 Summary of calculated results, $Re = 6 \times 10^6$.

$$\partial_\tau \hat{Q} + \partial_\xi \hat{E} + \partial_\eta \hat{F} = Re^{-1} \partial_\eta \hat{S} \qquad (1a)$$

where

$$\hat{Q} = J^{-1} \begin{bmatrix} \rho \\ \rho u \\ \rho v \\ e \end{bmatrix} .$$

$$\hat{E} = J^{-1} \begin{bmatrix} \rho U \\ \rho u U + \xi_x p \\ \rho v U + \xi_y p \\ (e + p)U - \xi_t p \end{bmatrix} \quad , \quad \hat{F} = J^{-1} \begin{bmatrix} \rho V \\ \rho u V + \eta_x p \\ \rho v V + \eta_y p \\ (e + p)V - \eta_t p \end{bmatrix} \qquad (1b)$$

$$\hat{S} = J^{-1} \begin{bmatrix} 0 \\ \mu(\eta_x^2 + \eta_y^2)u_\eta + (\mu/3)\eta_x(\eta_x u_\eta + \eta_y v_\eta) \\ \mu(\eta_x^2 + \eta_y^2)v_\eta + (\mu/3)\eta_y(\eta_x u_\eta + \eta_y v_\eta) \\ \kappa Pr^{-1}(\gamma - 1)^{-1}(\eta_x^2 + \eta_y^2)\partial_\eta a^2 \\ \quad + \mu(\eta_x^2 + \eta_y^2)(u^2 + v^2)_\eta/2 \\ \quad + (\mu/3)(\eta_x u + \eta_y v)(\eta_x u + \eta_y v_\eta) \end{bmatrix} \qquad (1c)$$

and U and V are the contravariant velocities along the ξ and η directions, given by

$$U = \xi_t + \xi_x u + \xi_y v$$
$$V = \eta_t + \eta_x u + \eta_y v \qquad (2)$$

The generalized coordinate system

$$\xi = \xi(x,y,t)$$
$$\eta = \eta(x,y,t) \qquad (3)$$
$$\tau = t$$

allows the boundary surfaces in the physical plane to be mapped into rectangular surfaces in the computational domain, as illustrated in the upper part of Fig. 3. This transformation simplifies the application of the boundary conditions in the computational domain and allows grid points to be clustered in the physical plane in regions of high gradients. The metrics ξ_t, ξ_x, etc., in Eq. (1) are formed from the derivatives of x_τ, x_ξ, etc., and the Jacobian of the transformation given by Eq. (3).

The pressure, density, and velocity components are related to the energy per unit volume by the equation of state for a perfect gas,

$$e = \frac{p}{(\gamma - 1)} + \frac{\rho}{2}(u^2 + v^2) \qquad (4)$$

The effective dynamic viscosity $\mu = \mu_L + \mu_T$ is typically comprised of a constant (molecular) value, μ_L, plus a computed turbulent eddy viscosity, ν_T/ρ, as discussed below.

Zero velocity is imposed as a boundary condition on the body; the thermodynamic variables at the body are derived from adiabatic wall conditions and the conditions $\partial p/\partial n = 0$ and $\partial \rho/\partial n = 0$ at the wall. The condition of uniform flow at infinity is approximated at the outer boundary of the computational domain by a nonreflective characteristic-like boundary procedure, with the additional stipulation that the velocities at these outer boundaries include the induction effects of the circulation (or lift) of the body. That is, the velocity field due to a compressible potential vortex of strength $\Gamma = (1/2)U_\infty c C_L$, where C_L is the lift generated by the airfoil, is superimposed at the outer boundary as a perturbation to the uniform free stream. The effectiveness of this circulation correction in the ARC2D code was demonstrated in Ref. 7 for inviscid calculations, and we verified the process for viscous flows by numerical experiments in which the distance to the outer boundary was varied from 6 to 48 chords. Within these bounds, the lift and drag were found to be constant to within 0.5% and 3%, respectively.

Approximations in the Viscous Regions

At the Reynolds numbers of interest in most helicopter applications, the effects of viscosity are concentrated near rigid boundaries and in wake regions. Furthermore, the flow gradients in the viscous layers of interest are generally much larger in the direction normal to the body than they are along the body. Therefore, it often suffices to neglect the "streamwise" viscous terms in the governing equations (see Eq. (1)). This "thin-layer" approximation is similar to the classical boundary-layer approximation, but the normal momentum equation is retained and solved. Thus, the pressure is allowed to vary across the viscous layer. Blottner[10] has recently discussed the thin-layer approximation in detail.

The thin-layer approximation can break down for low Reynolds numbers and in regions of massive flow separation. However, it affords significant computational economy. The resultant equations are slightly simpler; but more importantly, grid systems can be used that concentrate grid lines near the body, with fine grid spacing in the normal direction and relatively coarse grid spacing along the body (see Fig. 3). For the flow conditions considered in this paper, we feel it is

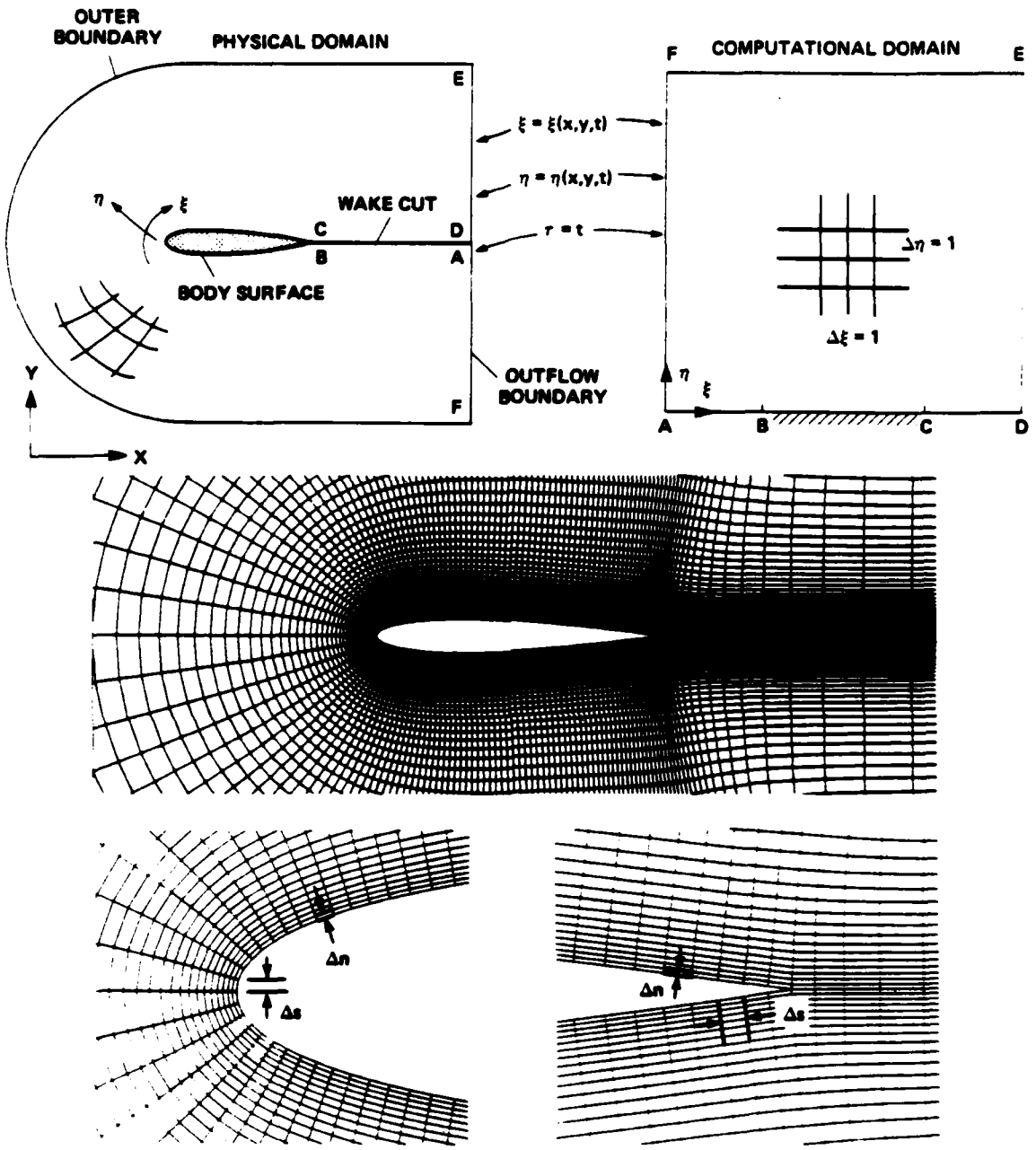

Fig. 3 Computational grids.

far more cost effective to neglect the streamwise viscous terms and to concentrate the grid along the body as shown in Fig. 3, than it would be to solve the full Reynolds-averaged Navier-Stokes equations with more nearly equal clustering of grid points in both the normal and streamwise directions.

The algebraic mixing-length model of Baldwin and Lomax[11] is used to approximate the effects of turbulence via the turbulent eddy viscosity, ν_T. As discussed in Refs. 11 and 12, the model consists of an inner layer that is governed by the Prandtl mixing length with van Driest damping, and an outer layer that follows the Clauser approximation. Computed vorticity is used in defining the reference mixing length. The Baldwin-Lomax model was designed specifically for use with the thin-layer approximation, and it is likewise suspect

for massively separated flows. Therefore, we have not attempted to calculate $C_{L_{max}}$, for example.

The ARC2D code can be applied to either laminar or turbulent flows, but transition to turbulence is not modeled. Therefore, transition point locations on the body have to be specified, or else determined by separate empiricism, as was done in the recent study by Mehta, Chang, and Cebeci[12] using ARC2D. Transition was fixed arbitrarily at $x/c = 0.01$ on both the upper and lower surfaces of the airfoil for all the cases presented in this paper. A limited study of transonic cases with other transition locations showed the lift and pitching moment to be relatively insensitive to this parameter, but the drag generally decreased with increasing x_T, as would be expected.

Computational Grids

Body-conforming grids of both the "O" and "C" topology were used and evaluated, with the C-topology illustrated in Fig. 3 generally converging to grid-independent values with fewer grid points or with fewer iterations. For most of the calculations shown in this paper, a variation of the hyperbolic grid-generation scheme of Barth, Pulliam, and Buning[13] was used, typically with 193 points in the ξ direction (72 points on each surface of the airfoil and 25 in the wake) and 64 points in the η direction. The outer boundary was normally placed 6 chords from the airfoil. The grid shown in Fig. 3 is for illustrative purposes only; the grid spacing shown near the body is much coarser than the ones we actually used.

The location of the outer boundary was found to be relatively unimportant when the circulation correction was used, as noted earlier. However, the grid spacing near the body is important, especially with regard to the drag coefficient. Whereas we found the lift to be essentially independent of the normal spacing, Δn, for minimum values less than about 0.0004, we were obliged to reduce Δn_{min} to about 0.00002 for reasonably reliable drag results.

The dependence on the spacing along the body, Δs, was less pronounced, but it was necessary to cluster grid points in the leading and trailing edge regions. Minimum values of $\Delta s = 0.002$ at the leading edge and 0.005 at the trailing edge were necessary to resolve the flow gradients near the nose and to attain regular behavior at the trailing edge. The Δs spacing was increased to approximately 0.025 at midchord. This spacing caused the computed shock waves to be smeared somewhat, but the aerodynamic coefficients were affected little by this.

Numerical Algorithm and Characteristics

The numerical method used to solve Eq. (1) is an alternating-direction fully implicit (ADI), approximate-factorization scheme, described in detail in Refs. 5-7. We used the Method 3 option, i.e., scalar pentadiagonal inversion,[6] of ARC2D-Version 1.50. The finite-difference approximations to Eq. (1) are solved as a series of time-like iterations, with the steady state approached asymptotically. However, for computational efficiency, the time step Δt is varied throughout the computational domain and with iteration number, so that the intermediate results are not "time accurate." Thus this variable time step is a numerical parameter that can be varied by the user of the code to enhance numerical stability and to accelerate the convergence.

Another numerical parameter that can be varied by the user is the artificial, or numerical, dissipation. Fourth-order implicit and explicit nonlinear dissipation terms are added to improve the nonlinear stability of the algorithm and to enhance its convergence, especially for transonic flows with shock waves.

We found by numerical experimentation that values of Δt and the dissipation coefficients close to the default values were satisfactory in most cases, although the cases with the largest separated zones required special treatment. Also, the grid spacing at the body was altered for the cases at the extreme values of Reynolds number. However, the convergence histories shown in Fig. 4 are representative of most of the results given in this paper. The engineering quantities of interest (i.e., lift, drag, and pitching-moment coefficients) normally converged to within 1% of their final values within about 1200 iterations, or approximately 5 min CPU time on the Ames Cray XM-P supercomputer. However, we always carried the calculations well beyond that point, until the residuals had dropped another order of magnitude, as indicated in Fig. 4. The CPU times were about 0.31 sec/iteration for the 193 × 64 grid.

Finally, we have developed some subjective impressions of the overall accuracy of the computed results, which are based on our extensive numerical experiments and on comparisons with wind tunnel data, as discussed in the following section. As noted above, the calculations normally converged to engineering accuracy, and also to within the limits of the numerical errors, in about 1200 iterations. Apart from cases with massive separation, the results for lift appear to be less than 5% in error; as shown below, the calculations match or slightly overpredict the measured values of C_L. The absolute uncertainty in the calculated drag coefficient is higher, because of

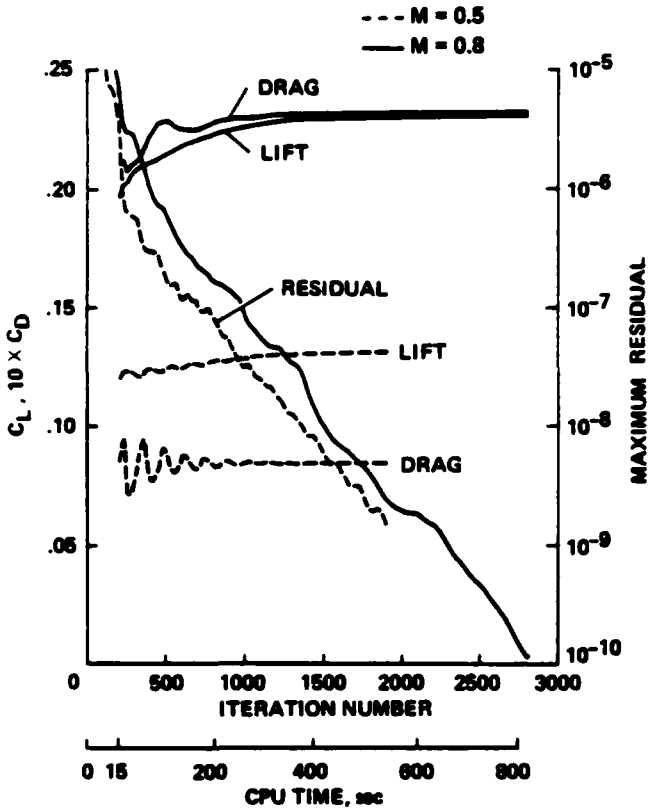

Fig. 4 Convergence history of a typical calculation.

the sensitivity to the grid, to the turbulence model, and to the transition location. The latter could account for up to ±0.0020 in C_D below drag divergence; otherwise, the errors are probably on the order of ±10% over the range of conditions considered herein. Our estimates of the uncertainty in the pitching moment coefficient are even more speculative: the greater of either C_m = ±0.005 or ±10%. While these uncertainty estimates are comparable to those of the best modern wind tunnels, they are not as low as the aircraft industry would like.[14]

Results and Discussion

As indicated in Fig. 2, approximately 90 combinations of airfoil, Mach number and angle of attack were computed, mostly at $Re = 6 \times 10^6$. The results are summarized in this section.

Experimental Data for Comparison and Validation

As noted earlier in connection with Table 1, wind tunnel results differ, according to the particular characteristics of each facility. For the purposes of this paper, data for the NACA 0012 airfoil from many sources have been screened and correlated, and those data from Refs. [1] and [15-22] have been assembled in Fig. 5. These sources include data that are considered to be virtually interference-free,[16] results which have been polished with the latest state of the art in wall-correction techniques,[17] a recent set of detailed measurements of exceptional quality, but which require significant angle-of-attack corrections,[18] and a benchmark data set from wartime Germany.[19] Also shown are representative results that are commonly used in the helicopter industry.[1,15,20-22] The Reynolds numbers vary from

- ✳ = Gregory and Wilby,[15] NPL 36 in. × 14 in. trip
- ⊕ = Vidal et al.,[16] Calspan 8 ft; trip
- ⊕ = Harris,[18] Langley 8 ft TPT; trip
- □ = Noonan and Bingham,[20] Langley 6 in. × 28 in.; no trip
- ⊞ = Noonan and Bingham,[20] Langley 6 in. × 28 in.; trip
- Δ = Prouty,[1] Lockheed 15 in. × 48 in. 2-D
- ⊠ = Gumbert and Newman,[17] Langley 0.3-m Cryogenic
- ▽ = Gothert,[19] DVL 2.7-m
- ○ = Jepson,[21] Tanner,[22] Lizak,[15], UTRC 8 ft
- ◇ = Jepson,[21] DTNSRDC 7 ft × 10 ft

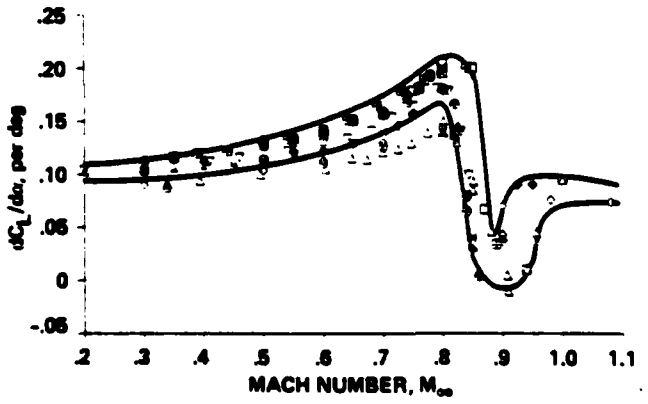

Fig. 5 Experimental results for the NACA 0012 airfoil.

approximately 10^6 to 10^7, and transition is both fixed and free.

In Fig. 5 and in several subsequent figures, the shaded bands are our assessments and interpretations of the limits of this aggregate of data; that is, the extent to which one may reasonably claim to know the force and moment characteristics of the NACA 0012 profile in practice. Some data have been discounted, for example, the low values of C_{L_α} from Refs. 1 and 21, which are probably contaminated by wall-interference effects. Also, the Calspan[16] values of drag coefficient at low Mach number appear to be too high, perhaps due to the type of boundary layer trip that was used. In the rest of this paper, our calculated results will be compared with experimental data bands that have been screened from Refs. 1 and 15-22 in this manner. It must be emphasized that the validity of the calculations can only be established to tolerances within these limits, and that no single experiment exists that is satisfactory for code validation.

Results for the NACA 0012

The numerical results for the NACA 0012 profile as a function of Mach number and angle of attack are shown in Figs. 6-10. As noted in the description of the numerical method, these calculations were all performed at $Re = 6 \times 10^6$, and boundary layer transition was assumed to occur at $x/c = 0.01$. Figures 7-9 include the experimental data described above; also shown for reference are the results of a standard transonic small-disturbance inviscid code, LTRAN2.[8]

Strong nonlinear compressibility effects are evident in C_L and C_D as M_∞ increases; e.g., the well-known drag divergence at $M_\infty = 0.78$ and the abrupt reduction in lift for $M_\infty \geq 0.82$. The spread in $(L/D)_{max}$ is much greater, but a substantial reduction with increasing M_∞ is apparent. The present results tend to fall below the middle of the experimental band, probably because the transition point was chosen at $x/c = 0.01$.

It is clear that the airloads computed by the present ARC2D viscous code exhibit all the features that have been revealed by the experiments, and the values of the coefficients are approximately within the ranges of the measured ones. There are two relatively minor discrepancies: first, the computed values of C_L at subsonic Mach numbers tend to be slightly higher than the data; and second, the computed drag coefficients follow the upper extremity of the experimental band. On the other hand, the nonlinear inviscid computations predict even higher C_L at subsonic Mach numbers, and the inviscid results are

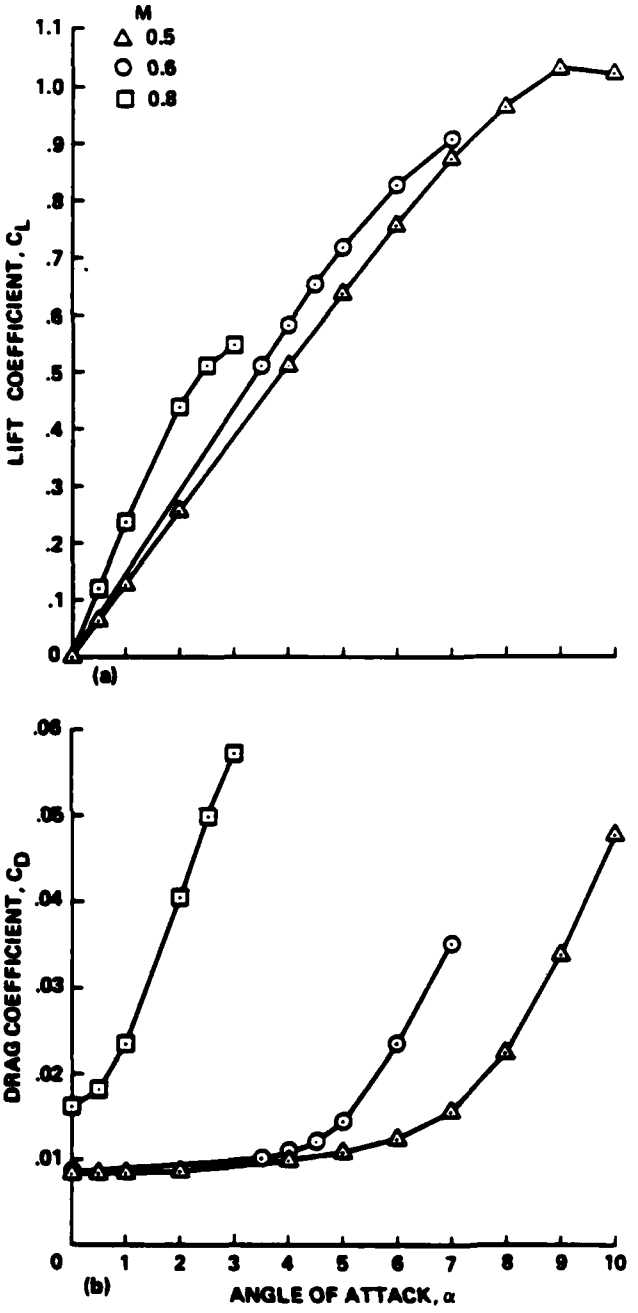

Fig. 6 Calculated results for the NACA 0012 airfoil with trip. a) Lift coefficient vs angle of attack; b) drag coefficient vs angle of attack.

completely unsatisfactory in the range $0.8 < M_\infty < 0.9$. This is associated with the shock wave-boundary layer interaction that dominates the real flow, as shown below.

As is well known, the drag divergence is related to the formation of shock waves on the airfoil for $M_\infty \geq 0.78$. Pressure distributions

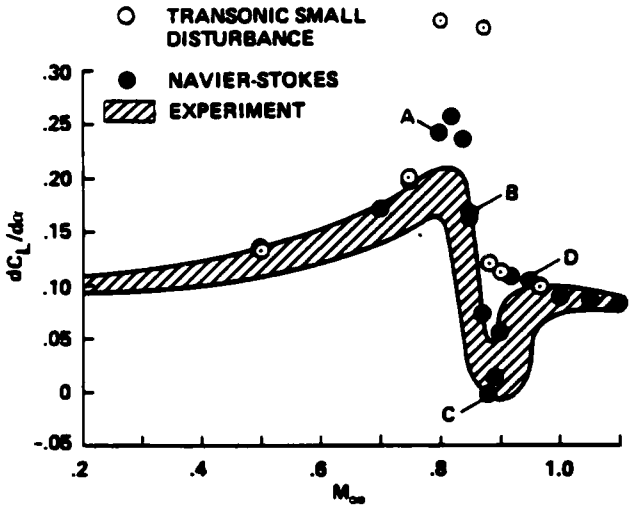

Fig. 7 Comparison of lift-curve slope for the NACA 0012 airfoil.

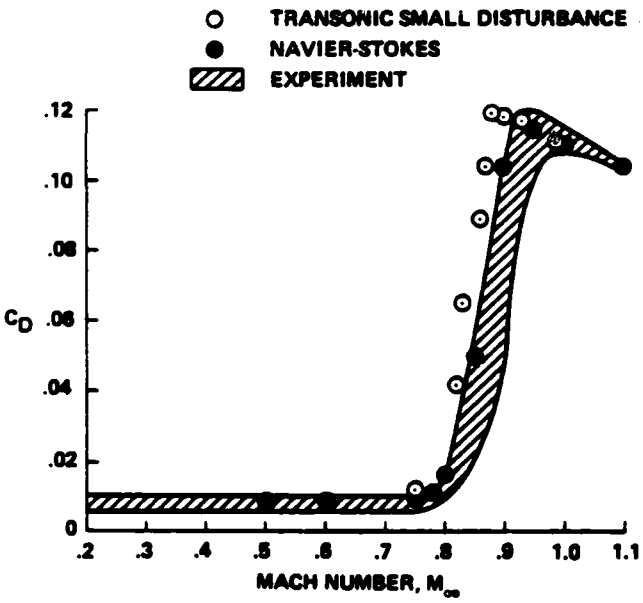

Fig. 8 Comparison of drag at zero lift for the NACA 0012 airfoil.

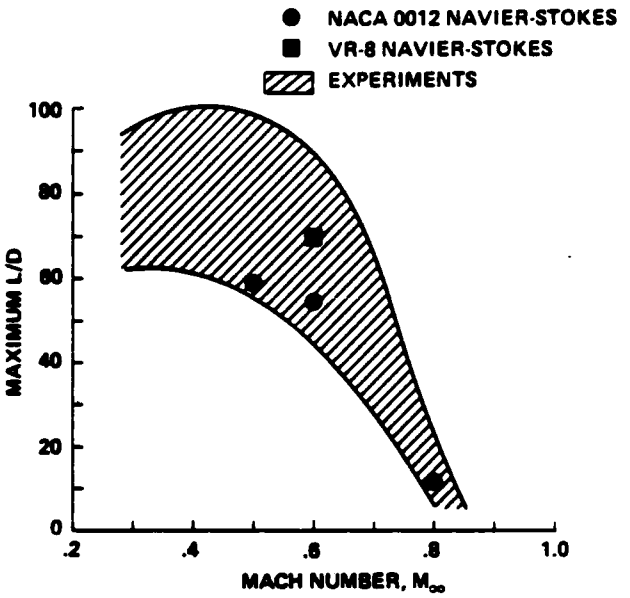

Fig. 9 Comparison of maximum lift-to-drag ratios.

and boundary-layer information that help explain the highly nonlinear behavior of C_L in Fig. 7 are shown in Fig. 10, corresponding to Points A-D in Fig. 7. Figure 10 illustrates the buildup of shock strength and shock wave/boundary layer interaction with increasing Mach number.

First, a small separation bubble appears on the upper surface at $M_\infty = 0.80$, and although the lift is greater than predicted by linear theory, it is significantly below the nonlinear inviscid value. At $M_\infty = 0.85$, the interaction between the shock wave and the boundary layer produces extensive separation on the upper surface and a small separation bubble on the lower surface, causing a further reduction in lift-curve slope. This trend continues up to $M_\infty = 0.88$ where, according to the viscous calculations, a minimum value of $dC_L/d\alpha = 0$ occurs. At this point, the upper-surface shock wave is stronger than the lower, but the separated viscous layer pushes it farther upstream; consequently, the net lift is approximately zero, but the pitching moment derivative (not shown) attains a maximum positive value of $dC_M/d\alpha = 0.04$/deg.

At higher Mach numbers, the shock waves on both surfaces move to the trailing edge, the viscous effects become relatively unimportant, and the rates of change of C_L, C_D, and C_M with M_∞ become much less. No further significant qualitative changes occur up to the maximum Mach number considered, $M_\infty = 1.10$. It is interesting to note that the inviscid code becomes surprisingly accurate again for $M_\infty \geq 0.94$.

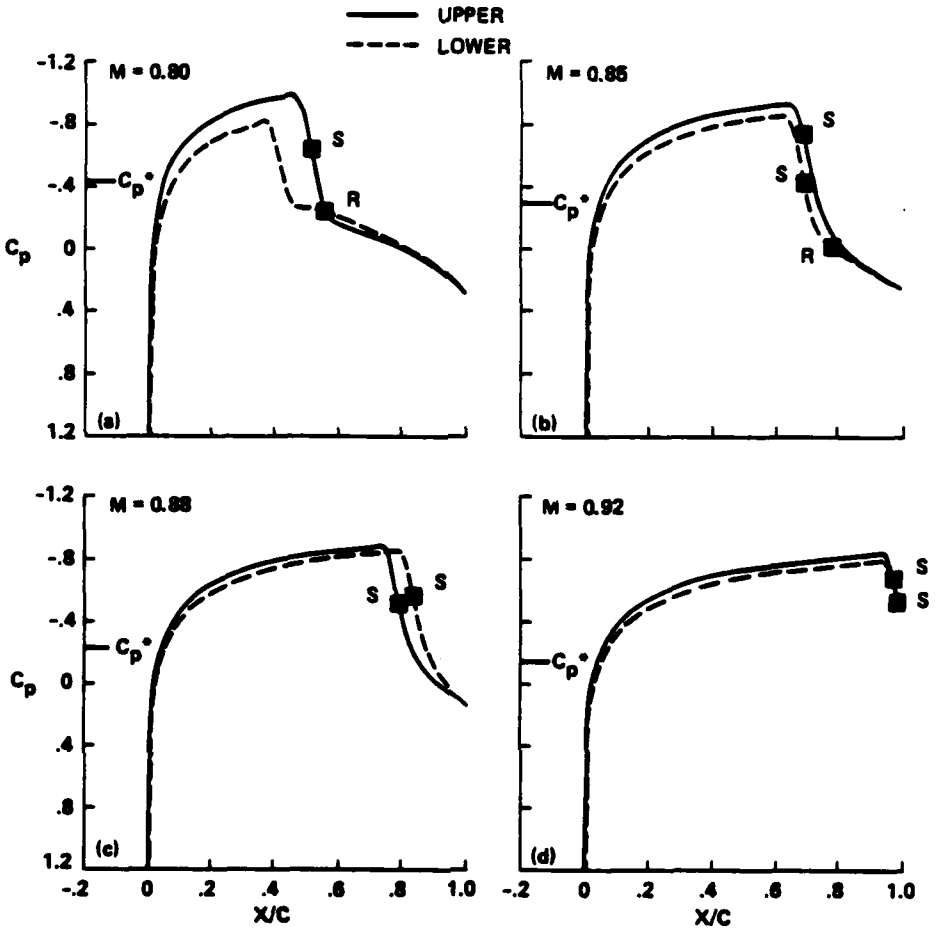

Fig. 10 Pressure distributions for the NACA 0012 airfoil; $\alpha = 1/2°$, $Re = 6 \times 10^6$, S denotes boundary-layer separation, R reattachment.

Correlation of Transonic Drag Characteristics

Recently F. D. Harris (private communication) reminded the authors of Spreiter's[23] work with similarity parameters as an aid in correlating the drag due to shock waves in the transonic regime. The basic transonic similarity parameters are

$$\bar{C}_D = \frac{C_{D_p} M_\infty^{2/3} (\gamma + 1)^{1/3}}{(t/c)^{5/3}} \tag{5}$$

$$\bar{M} = \frac{M_\infty^2 - 1}{M_\infty^{4/3} (t/c)^{2/3} (\gamma + 1)^{1/3}} \tag{6}$$

where C_{D_p} is the increment in drag coefficient above the subsonic level, γ is the specific heat ratio, and t/c is the airfoil thickness ratio. Harris (private communication) has found $\bar{C}_D$ to correlate approximately uniquely with $\bar{M}$ and the position of the maximum airfoil thickness.

Figure 11 shows that our calculated results of $\bar{C}_D$ versus $\bar{M}$ correlate well for the four airfoils considered. Also shown in the figure are Harris' correlation of a number of finite wing tests, and the band of data from Refs. 1 and 15-22. As noted earlier in connection with Fig. 8, our numerical results follow the upper limit of the available measurements.

Results for the Vertol VR-8 Airfoil

The transonic pitching moment behavior has particularly important consequences on the advancing blade of a rotor in high-speed forward flight. Large torsional loads can be created by the rapid growth in C_M that occurs when the aerodynamic center of pressure shifts rearward in

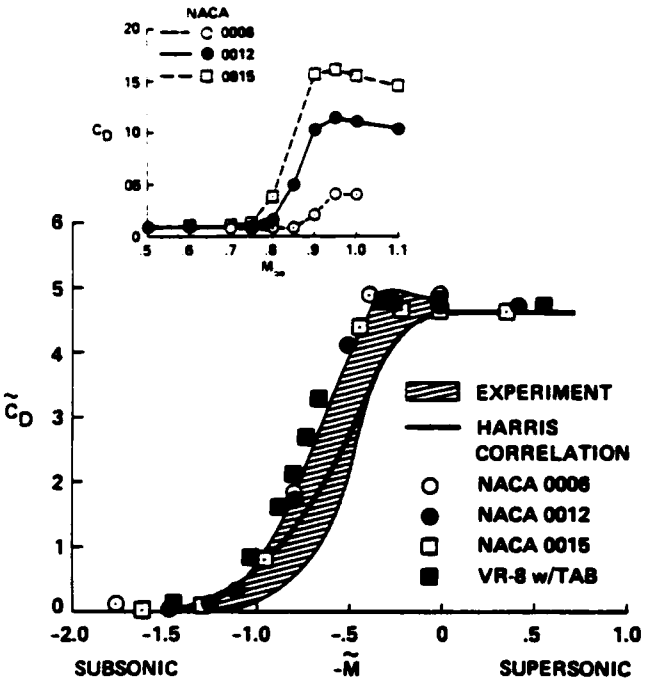

Fig. 11 Correlation of drag results in transonic similarity parameters.

the transonic regime, a phenomenon known as "Mach tuck."

Figures 12 and 13 show the computed pitching moment behavior and drag coefficient of the VR-8 section at zero lift compared with wind tunnel measurements.[15] The calculations were performed both at a fixed Reynolds number, corresponding to the NACA symmetrical-airfoil results described above, and at the varying Reynolds numbers of the experiment, $8\text{-}13 \times 10^6$. Transition was assumed at $x/c = 0.01$ in all cases. As shown in the figures, the results are insensitive to Reynolds number in this limited range.

The large Mach-tuck dip that occurs for $0.8 < M_\infty < 0.9$ is clearly evident in Fig. 12. The calculated results shown in Figs. 12 and 13 are in excellent agreement with the measurements, except for the maximum negative value of C_M and the Mach number at which it occurs. The values of $(L/D)_{max}$ at $M_\infty = 0.60$ and $\bar{C}_D$ versus $\bar{M}$ were shown earlier in Figs. 9 and 11, respectively. In both cases, the aerodynamic performance is superior to that of the NACA 0012.

The pressure distributions and boundary-layer information relevant to the nonlinear behavior shown in Figs. 12 and 13 are given in Fig. 14. As in the NACA 0012 results considered earlier, the figure illustrates the buildup of shock strength

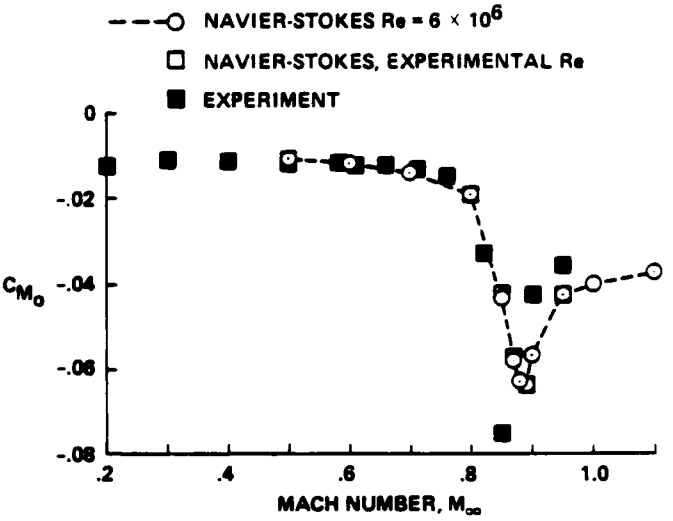

Fig. 12 Pitching moment vs Mach number for the VR-8 airfoil at $C_L = 0$.

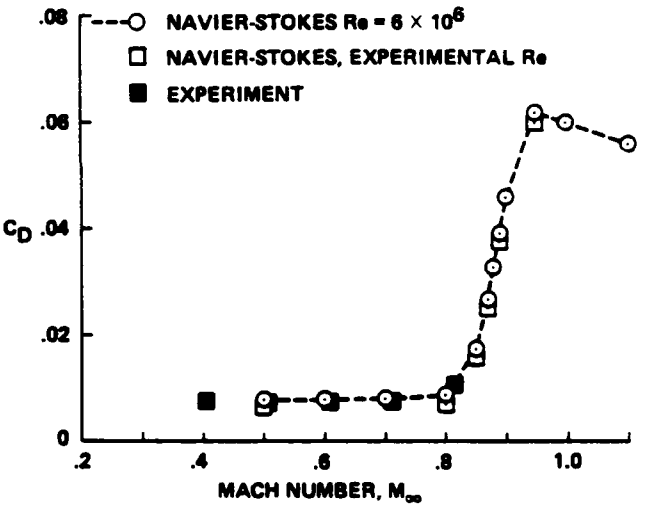

Fig. 13 Drag coefficient vs Mach number for the VR-8 airfoil at $C_L = 0$.

and shock wave/boundary layer interaction with increasing Mach number. However, the actual pressure distributions are considerably different from those shown in Fig. 10. The cases between $M_\infty = 0.85$ and 0.90, which encompass the peak in $-C_M$, coincide with the maximum amount of shock-induced separation on the airfoil. The disagreement with the experimental data for $0.85 < M_\infty < 0.90$ could be due to errors in modeling the boundary layer transition, as the experimental transition characteristics were not specified. On the other hand, the spread in the available data on the NACA 0012 airfoil (e.g., Figs. 5, 7, 8, and 9) suggests that it is unwise to place too much faith in a single experiment.

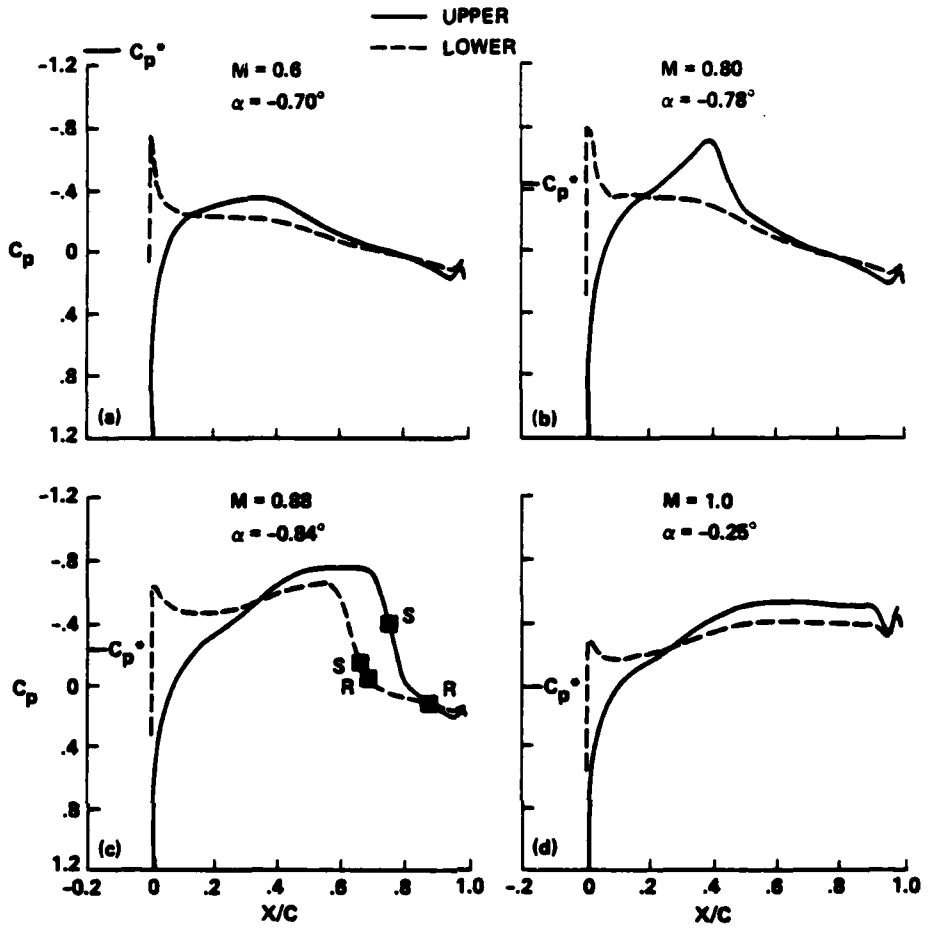

Fig. 14 Pressure distributions for the VR-8 airfoil at $C_L = 0$; S denotes boundary-layer separation, R reattachment.

Effects of Reynolds Number

Subject to the limitations of the empirical models for turbulence and transition, the computations can be run over virtually an unlimited range of Reynolds numbers. Representative subsonic and transonic results for the NACA 0012 airfoil between 1 and 100 × 10^6 are shown in Fig. 15 for transition fixed at x/c = 0.01. The results show a monotonic decrease in C_D with increasing Re, whereas the lift monotonically increases.

The pressure distributions corresponding to the $M_\infty = 0.80$ case are given in Fig. 16. These results are all qualitatively the same, but the shock-induced boundary-layer separation is a strong function of Reynolds number. For example, the separation zone on the upper surface at $Re = 10^6$ extends from the shock wave to the trailing edge, whereas it is only a short bubble at $Re = 10^7$, and there is no separation at $Re = 10^8$. It is interesting to note that although the subsonic drag coefficients are considerably

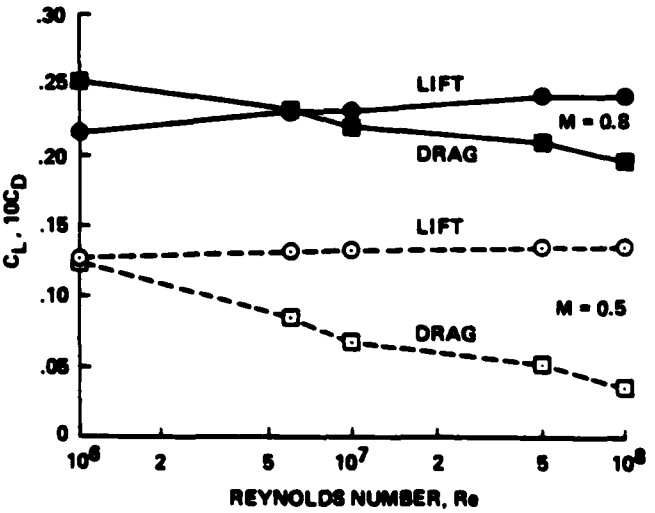

Fig. 15 Effect of Reynolds number on lift and drag; NACA 0012, $M_\infty = 0.5$ and 0.8, $\alpha = 1°$.

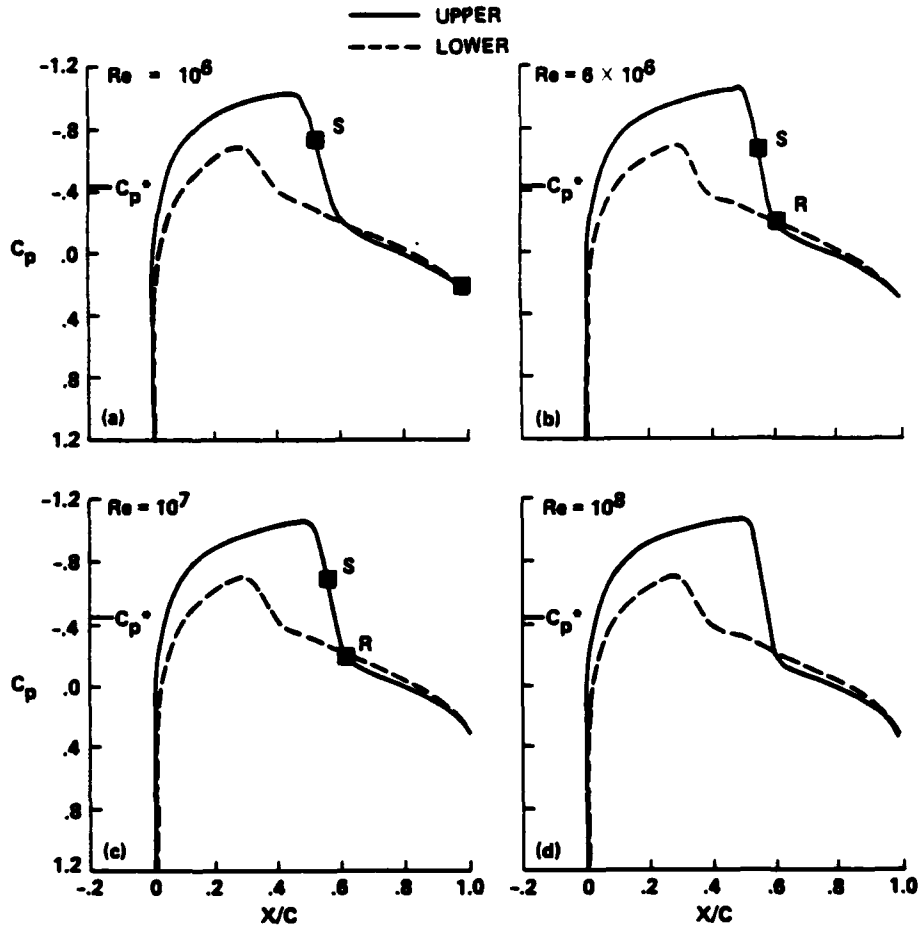

Fig. 16 Pressure distributions on the NACA 0012 airfoil at $M = 0.80$ and $\alpha = 1°$.

less than the transonic values, the percentage change with Re is actually greater.

Summary and Conclusions

In this paper, we have applied a new aerodynamic tool to the study of helicopter airfoil characteristics. We have shown that the computed airloads reproduce completely the experimental behavior of representative airfoils across the transonic regime. In addition, the computational details of the flow fields, the surface pressure distributions, and the viscous-layer characteristics enable us to trace the evolution of the physical changes that occur as M_∞ or Re increases. Descriptions of the complicated development of shock waves, shock wave-boundary layer interaction, and shock-induced separation supplement the information that has been obtained heretofore in wind tunnels.

In validating our calculations and assessing the accuracy of the results, including extensive grid-refinement studies and comparisons with data from numerous wind tunnels, we have defined more precisely the capabilities and limitations of the code ARC2D. This important aspect of the investigation has also revealed ways that the computations can complement wind-tunnel tests, by providing flow-field details that are difficult to measure and by extending the range of flow parameters beyond the capabilities of existing wind tunnels. The code has now progressed from a purely research stage to almost a production stage, where it can be run by specialists in the helicopter industry.

We claim that the numerical results presented in this paper are as accurate as contemporary experimental measurements, and that new physical insights into transonic airfoil behavior can be obtained from the details of these calculations. However, we emphasize that these and similar emerging CFD capabilities represent new tools to complement experimental measurements, rather than substitutes for wind tunnel testing. Each

approach has its unique capabilities, limitations, economics, and manpower requirements. The future of helicopter technology is best served by an intelligent combination of the two.

References

1. Prouty, R., "Aerodynamics," Rotor and Wing International, Aug. 1984, pp. 17-22.

2. Prouty, R., "Aerodynamics," Rotor and Wing International, Dec. 1983, pp. 9-13.

3. McCroskey, W. J., McAlister, K. W., Carr, L. W., and Pucci, S. L., "An Experimental Study of Dynamic Stall on Advanced Airfoil Sections," NACA TM-84245, July 1982.

4. McCroskey, W. J., "Round Table Discussion on 'Wall Interference in Wind Tunnels,'" AGARD Conference Proceedings CP-335, May 1982.

5. Pulliam, T., "Euler and Thin Layer Navier-Stokes Codes ARC2D and ARC3D," Computational Fluid Dynamics User's Workshop, Univ. Tenn. Space Inst. E02-4005-023-84, Tullahoma, Tenn., May 1984.

6. Pulliam, T. H. and Steger, J. L., "Recent Improvements in Efficiency, Accuracy, and Convergence for Implicit Approximate Factorization Algorithms," AIAA Paper 85-0360, Reno, Nev., Jan. 1985.

7. Steger, J. L., "Implicit Finite-Difference Simulation of Flow about Arbitrary Two-Dimensional Geometries," AIAA Journal, Vol. 16, No. 7, July 1978, pp. 679-686.

8. Ballhaus, W. F., Jr., and Goorjian, P. M., "Implicit Finite-Difference Computations of Unsteady Transonic Flows about Airfoils," AIAA Journal, Vol. 15, Dec. 1977, pp. 1728-1735.

9. Dougherty, F. C., Holst, T. L., Gundy, K. L., and Thomas, S. D., "TAIR--A Transonic Airfoil Analysis Computer Code," NASA TM-81296, May 1981.

10. Blottner, F. G., "Significance of the Thin-Layer Navier Stokes Approximation," 3rd Symposium on Numerical and Physical Aspects of Aerodynamic Flows, California State University, Long Beach, Calif., Jan. 1985.

11. Baldwin, B. S. and Lomax, H., "Thin Layer Approximation and Algebraic Model for Separated Turbulent Flows," AIAA Paper 78-257, Huntsville, Ala., Jan. 1978.

12. Mehta, U., Chang, K. C., and Cebeci, T., "Relative Advantages of Interactive and Thin-Layer Navier Stokes Procedures," 3rd Symposium on Numerical and Physical Aspects of Aerodynamic Flows, California State University, Long Beach, Calif., Jan. 1985.

13. Barth, T. J., Pulliam, T. H., and Buning, P. G., "Navier-Stokes Computations for Exotic Airfoils," AIAA Paper 85-0109, Reno, Nev., Jan. 1985.

14. Steinle, Jr., F. W. and Stanewsky, E., "Wind Tunnel flow Quality and Data Accuracy Requirements," AGARD Advisory Report AR-184, 1982.

15. Dadone, L. U., "U.S. Army Helicopter Design DATCOM. Vol. I: Airfoils, Final Report," NASA CR-153247, May 1976.

16. Vidal, R. J., Catlin, P. A., and Chudyk, D. W., "Two-Dimensional Subsonic Experiments with an NACA 0012 Airfoil," Calspan Report RK-5070-A-3, Calspan Corp., Buffalo, N.Y., Dec. 1973; also Paper No. 11, AGARD Conference Proceedings CP-174, Oct. 1975.

17. Gumbert, C. R. and Newman, P. A., "Validation of a Wall Interference Assessment/Correction Procedure in the Langley 0.3-m Transonic Cryogenic Tunnel," AIAA Paper 84-2151, Seattle, Wash., Aug. 1984.

18. Harris, C. D., "Two-Dimensional Aerodynamic Characteristics of the NACA 0012 Airfoil in the Langley 8-foot Transonic Pressure Tunnel," NACA TM-81927, Apr. 1981.

19. Gothert, B., "Airfoil Measurements in the DVL High-Speed Wind Tunnel (2.7-meter Diameter)," NACA TM-1240, June 1949.

20. Noonan, K. W. and Bingham, G. J., "Two-Dimensional Aerodynamic Characteristics of Several Rotorcraft Airfoils at Mach Numbers from 0.35 to 0.90," NASA TM X-73990, Jan. 1977.

21. Jepsen, W. D., "Two Dimensional Test of Four Airfoil Configurations with an Aspect Ratio of 7.5 and a 16 inch Chord up to a Mach Number of 1.1," Sikorsky Report SER-50977, Sikorsky Aircraft, Stratford, Conn., Apr. 1977.

22. Tanner, W. H., "Charts for Estimating Rotary Wing Performance in Hover and at High Forward Speeds," NACA CR-114, Nov. 1964.

23. Spreiter, J. R., "On the Application of Transonic Similarity Rules to Wings of Finite Span," NACA Technical Report 1153, 1953.

END

FILMED

12-85

DTIC